LIMNOLOGY
and
OCEANOGRAPHY: METHODS

ASLO

*Limnol. Oceanogr.: Methods* 23, 2025, 652–672

doi: 10.1002/lom3.10711

NEW METHODS

# Characterizing the response time of unpumped oxygen optodes for profiling applications

**Ellen Park**,[1,2]* **David Nicholson**,[2]* **Mathieu Dever**,[2,3] **Dariia Atamanchuk**,[4] **Clark Richards**[4,5]

[1]MIT-WHOI Joint Program in Oceanography, Woods Hole, Massachusetts, USA; [2]Department of Marine Chemistry & Geochemistry, Department of Physical Oceanography, Woods Hole Oceanographic Institution, Woods Hole, Massachusetts, USA; [3]RBR Ltd, Ottawa, Ontario, Canada; [4]Department of Oceanography, Dalhousie University, Halifax, Nova Scotia, Canada; [5]Department of Fisheries and Oceans Canada, Bedford Institute of Oceanography, Dartmouth, Nova Scotia, Canada

## *Abstract*

The response times of the Aanderaa 4330, Aanderaa 4330 WTW, RBR*coda* T.ODO|slow, and PyroScience PICO-O2-SUB were evaluated in the laboratory over a range of profiling speeds at two temperatures. The PyroScience PICO-O2-SUB had the fastest response time (1–4 s), followed by the RBR*coda* T.ODO|slow (∼ 15–35 s), Aanderaa 4330 (∼ 30–60 s), and Aanderaa 4330W (∼ 50–100 s). This study provides recommendations on improving the quality of oxygen data from optodes in profiling applications by additionally assessing the impact of response time testing setups, thermal inertia effects, and foil types on sensor response times. This study provides a new response time function based on physical principles to predict response time for these four optode types.

Oxygen is an important molecule necessary for maintaining healthy ecosystems both on land and in the ocean. In the ocean, oxygen measurements have been and continue to be used to quantify a variety of processes, such as ecosystem productivity and respiration (Karstensen et al. 2008; Plant et al. 2016; Yang et al. 2019), ventilation (Koelling et al. 2022), and ocean deoxygenation (Oschlies 2021; Sharp et al. 2023). The oxygen content of the ocean has been declining due to climate-related feedbacks (Oschlies 2021; Schmidtko et al. 2017). This necessitates close monitoring of oxygen levels in the global ocean. Oxygen is one of the essential ocean variables recognized by the Global Ocean Observing System, which requires a measurement accuracy $< 2\,\mu$M to sufficiently constrain the phenomenon (IOCCP 2017).

Historically, ocean oxygen measurements have been made through Winkler titrations of water samples (Winkler 1888). While Winkler oxygen measurements can have a precision and accuracy of $\pm$ 0.15 $\mu$mol kg$^{-1}$ (Langdon 2010), ship-based measurements are laborious, costly, limited in both space and time, and often exhibit a seasonal sampling bias (Riser et al. 2016). Over recent decades, dissolved oxygen sensing from autonomous platforms has been dominated by the use of oxygen optodes, which can have an accuracy of 2 $\mu$M (Tengberg et al. 2006), but this depends on the specific optode type (*see* Table 1) and can be reduced due to other factors, such as sensor drift, pressure effects, and the extent of biofouling.

Biogeochemical (BGC)-Argo, a global array of autonomously drifting profiling floats equipped with a suite of BGC sensors, has expanded oxygen measurements, in addition to other BGC measurements, across both space and time (Biogeochemical-Argo Planning Group 2016; Claustre et al. 2020). This has had a notable impact on observing the annual cycle in high latitude regions, like the Southern Ocean (Gray et al. 2018), and

*Correspondence: erpark@mit.edu; dnicholson@whoi.edu



**Associate editor:** Mike DeGrandpre

**Data Availability Statement:** Flume response time results, code to predict response times, and code to response time correct oxygen time series are available in the GitHub repository (https://github.com/ellenrpark/optode_response). The Argo data (WMO 690089 and 690090) used in this study are collected and made freely available by the International Argo Program and the national programs that contribute to it (https://argo.ucsd.edu; https://www.ocean-ops.org). The Argo Program is part of the Global Ocean Observing System. Float data from Gordon et al. (2020) are available at https://zenodo.org/records/3890240.

**Table 1.** Abbreviations for the four different optodes used in this study, along with their foil type, manufacturer reported response time, and the response time determined in this study.

| Optode type (abbreviation) | Foil material | Manufacturer accuracy | Manufacturer response time (s) | This study's response time (s) |
|---|---|---|---|---|
| Aanderaa 4330 (AA4330) | PreSens PSt3 | $< 2\ \mu$M | < 25* | ~ 50–100 |
| Aanderaa 4330W (AA4330\|WTW) | Xylem WTW FDO 701 | | < 30* | ~ 30–60 |
| RBR*coda* T.ODO\|slow (RBR\|SLOW) | PreSens PSt3 | Maximum of 2 $\mu$M or $\pm$ 1.5% | < 30† | ~ 15–35 |
| PyroScience PICO-O2-SUB, OEM version (PYRO-PICO) | PyroScience GmbH | $\pm$ 3 $\mu$M | < 3 s‡ | ~ 1–4 |

*Aanderaa Data Instruments AS (2024).
†RBR Ltd (2024).
‡PyroScience GmbH (2024).

has allowed for the creation of four-dimensional, gridded, observational BGC products (Sauzède et al. 2016; Sharp et al. 2023). The success of this float array to produce reliable and accurate data heavily relies on the proper characterization of sensors. A threshold and target accuracy (5 $\mu$mol kg$^{-1}$, 1 $\mu$mol kg$^{-1}$) and precision (2 $\mu$mol kg$^{-1}$, 0.5 $\mu$mol kg$^{-1}$) for oxygen measurements on this array is defined to meet the scientific objectives of the array and are also relevant for other process studies of interest to the scientific community (Grégoire et al. 2021; Gruber et al. 2010).

Oxygen, which is the most and longest measured BGC parameter on the BGC-Argo array (third overall to temperature and salinity), is measured using optodes. The most common optodes deployed are the unpumped Aanderaa 3830/4330, which has a reported accuracy < 2 $\mu$M, and the pumped Sea-Bird Electronics (SBE) 63, which has a reported accuracy of the larger of 3 $\mu$mol kg$^{-1}$ or $\pm$ 2%. These sensors have been well-characterized with respect to both their temperature and pressure dependence (Bittig et al. 2015a; Bittig et al. 2018; Miller et al. 2024; Tengberg et al. 2006), as well as their stability over time (Ren et al. 2023; Tengberg et al. 2006). Furthermore, since oxygen measurements from BGC-Argo floats have been made since 2010, a wide array of in situ calibration methods for these floats have been developed to correct for storage and sensor drift, such as using climatological oxygen (Takeshita et al. 2013) or in-air oxygen measurements (Bittig and Körtzinger 2017; Johnson et al. 2015), which have a 3% and 1% accuracy, respectively. The workflow for processing, quality-controlling, and reporting errors based on these methods for float oxygen data is well-documented and currently implemented across the BGC-Argo array (Thierry et al. 2021).

However, the sensor response time, which is how quickly a sensor responds to a change in the measured variable, is an important aspect of sensor characterization that has yet to be included in this workflow. This is significant as previous studies have shown that not accounting for this can lead to errors of 10–20 $\mu$mol kg$^{-1}$ or more in regions with strong oxygen gradients (Bittig and Körtzinger 2017; Cervania and Hamme 2024). Thankfully, the response time is a factor that can be controlled, but it requires careful assessment in the laboratory and must consider other factors such as sensor orientation, water temperature, and flow speed (Bittig et al. 2014).

For an oxygen optode, the response time depends on the diffusion of oxygen across a liquid boundary layer that forms at the sensor face, followed by the diffusion of oxygen into and through the sensor foil (Bittig et al. 2014). Previous studies, which examined optode response times both experimentally and theoretically using a two-layer stagnant diffusion model, found that the response time depends on flow speed, temperature, and, perhaps, deployment platform, such as on a float or glider, as this can affect the local flow regime (Bittig et al. 2014; Bittig and Körtzinger 2017). Specifically, the response time is faster at both higher flow speeds because the boundary layer is thinner and warmer temperatures because the rates of diffusion are faster. These previous studies also found that the boundary layer thickness is independent of temperature and depends only on flow speed for a given deployment platform, requiring that a velocity-boundary layer relationship must be determined for each deployment platform (Bittig et al. 2014; Bittig and Körtzinger 2017). However, the principles of fluid mechanics and mass transfer dictate that this boundary layer is not, in fact, independent of temperature, suggesting additional research is needed to reconcile these differences (Welty et al. 2014).

Careful characterization of the flow speed and temperature dependence of an optode's response time is important for BGC-Argo float applications, as floats profile at ~ 10 cm s$^{-1}$ over a wide range of temperatures. The oxygen optodes used on this array typically have a slow response (~ 30–80 s; Bittig et al. 2014) that, if not accounted for, can result in a measurement bias that is correlated with the oxygen gradient (Bittig et al. 2014; Bittig and Körtzinger 2017; Cervania and Hamme 2024), as demonstrated in Fig. 1, which shows idealized response time errors using a fixed response time of 75 s in the upper 1000 dbar of the ocean along the P18 GO-SHIP line where there is a strong oxygen gradient and a large oxygen deficient zone. This measurement error depends on both the

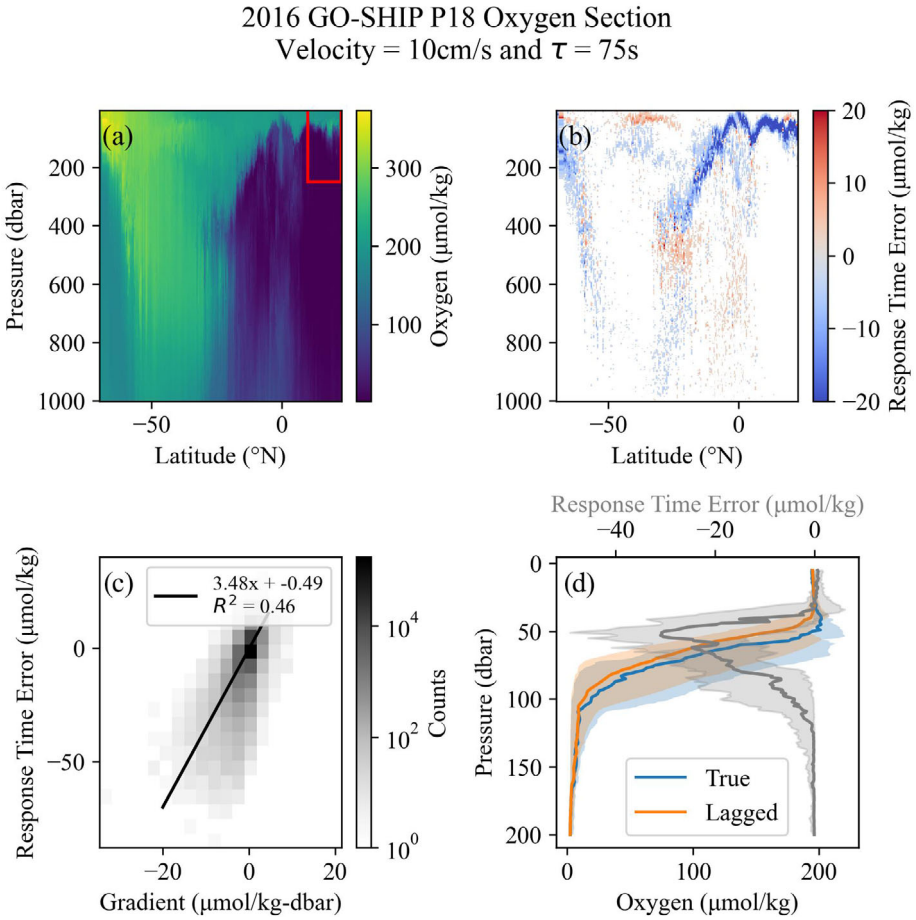


**Fig. 1.** (**a**) GO-SHIP P18 dissolved oxygen section (Rolf Sonnerup 2016). (**b**) Idealized response time error, using a profiling velocity of 10 cm $s^{-1}$ and a fixed response time of 75 s, defined as the difference between the lagged and true oxygen profiles. White regions are where the absolute value of the difference is less than or equal to 2 $\mu$mol $kg^{-1}$. (**c**) Response time error vs. local oxygen gradient. (**d**) Median oxygen profiles from all casts (True, blue) and idealized lagged profiles (Lagged, orange) north of 10°N (indicated by red box in (**a**)) with shading denoting 25$^{th}$ and 75$^{th}$ quantiles in the upper 250 dbar with the response time error profiles in gray.

response time and the local gradient, with the largest errors occurring when the sensor response time is slow and the oxygen gradient is large (Fig. 1b–d). While in many regions of the ocean, the response time error is comparable to the sensor accuracy (< 2 $\mu$mol $kg^{-1}$, white regions in Fig. 1b), this is not the case in regions with high vertical gradients in dissolved oxygen and temperature, such as the thermocline above oxygen deficient zones, where the errors can be far greater than 10 $\mu$mol $kg^{-1}$ (Cervania and Hamme 2024). Not accounting for slow sensor response in these regions can result in artifacts in annual net community production estimates from float oxygen at Ocean Station Papa, further highlighting the importance of accounting for these errors (Plant et al. 2016).

As the BGC-Argo fleet continues to expand to include a more diverse set of float manufacturers and sensors, ensuring proper characterization of all BGC sensors is of utmost importance. This study aims to quantify and assess the impacts of temperature and flow speed on the dynamic response time of four different unpumped oxygen optodes (Aanderaa 4330, Aanderaa 4330 WTW, RBR*coda* T.ODO|slow, PyroScience PICO-O2-SUB), which are or may become suitable for profiling float applications. The SBE63 is not considered in this study as its response time has already been characterized and has less uncertainty because it sits in a pumped flow path (Bittig et al. 2014; Bittig and Körtzinger 2017). The results from the response time experiments are used to create an empirical formula to calculate the response time in the field for each sensor based on a Reynolds-number-like value. Additionally, the impacts of sensing foils, sensor geometry, and thermal inertia effects are investigated in this study.

## Materials and procedures

### Oxygen optode sensing principles and design

Oxygen optodes are designed based on the principles of measuring luminescence quenching (*see* Bittig et al. 2018 for a more in depth explanation). A luminophore is excited by a specific wavelength of light, and the time it takes for the luminophore to decay back to its ground state is influenced by

the presence of oxygen. Specifically, the luminescence lifetime is reduced by the presence of oxygen. Optodes measure the phase shift of luminescence lifetime to the frequency of the modulated excitation light. This phase shift can then be converted to the partial pressure or concentration of oxygen via polynomial functions, such as the Stern-Volmer or modified Stern-Volmer equations (Uchida et al. 2008).

The luminophore, which is often a platinum porphyrin complex, is fixed in a membrane, which is the main component of the sensing foil (Staudinger et al. 2018; Tengberg et al. 2006). This sensing foil, in addition to the protective foil coating and sensor geometry, has an impact on the optode's response time and stability. The faster response time often comes at the expense of reduced sensor stability over time, so slower (typically referred to as standard) and more stable foils are thus preferred for long-term deployments on autonomous platforms, like BGC-Argo floats and long-term moorings. The sensing foils and varying manufacturer reported response times for the four different optodes (Aanderaa 4330, Aanderaa 4330W, RBR*coda* T.ODO|slow, PyroScience PICO-O2-SUB) are listed in Table 1. All optodes, except for the Aanderaa 4330 and RBR*coda* T.ODO|slow, use different sensing foils. The Aanderaa 4330W was chosen because the WTW foil, according to the manufacturer, has better stability and a lower pressure effect compared to the PSt3 foil, which has been well-characterized and widely used in practice until this point. The RBR*coda* T.ODO|slow and Aanderaa 4330 are generally the most widely used in the community. Finally, the PyroScience PICO-O2-SUB was chosen because of its fast response time (~ 3 s) and increased interest in the applications of its pH optode counterpart, the PICO-PH-SUB (Staudinger et al. 2018, 2019; Wirth et al. 2024).

The Aanderaa 4330 and RBR*coda* T.ODO|slow are reported to use the same PSt3 foil (PreSens GmbH) (*see* Table 1). The newer Aanderaa 4330W has the same sensor geometry but replaces the PSt3 foil with an in-house FDO701 foil (WTW, Xylem). Both Aanderaa optodes and the RBR optode have a sensor face that is angled at 45° to reduce the formation of a stagnation point during profiling and to avoid water droplets on the sensing foil during in-air calibration. The PyroScience PICO-O2-SUB with the OXCAP-SUB sensor cap does not have this 45° angle. Instead, the sensor face is flat with a protective guard.

### Flume response time characterization

The response times of four different commercial oxygen optodes were determined over a range of flow speeds corresponding to profiling float speeds at two different temperatures at the Aquatron Laboratory's flume tank at Dalhousie University in Halifax, Nova Scotia, Canada. Figure 2 shows the setup used for these experiments. The flume tank is approximately 50 cm wide × 50 cm tall and roughly 8 m long and was selected to emulate a profiling float traveling vertically through the water column. Flow speed and recirculation of water within the flume are controlled by a turbine. Baffling


**Fig. 2.** (**a**) Flume experimental response time setup with key components labeled. Insets show close ups of other key components of setup. (**b**) Suite of optodes on support structure mounted in the flume. (**c**) Suite of optodes on support structure equilibrating in the calibration bench's temperature-controlled jacketed water tank. (**d**) Suite of optodes on support structure equilibrating in calibration bench's temperature-controlled jacketed water tank with caps on. *See* Supporting Information Fig. S2 for an additional sketch of the flume setup.

at the upstream inlet of the flume is designed to produce laminar flow at constant velocity through the core of the flume. All sensors were kept approximately ~ 10–15 cm away from bottom and side boundaries (*see* Supporting Information Fig. S2 for additional schematic of the setup). This saltwater flume was previously used to characterize dynamic errors in CTDs (Dever et al. 2022).

The flume was filled with seawater from the Northwest Arm of Halifax Harbor (temperature: ~ 6°C, salinity: ~ 30, oxygen saturation ~ 100%). A Nortek Vector current velocimeter was installed upstream of the sensors to measure in situ velocity, and at least one reference CTD (RBR*concerto*$^3$) was placed downstream to measure the in situ temperature and salinity of the tank throughout the duration of the experiment. While there appeared to be no issues with the Nortek during the experiments, the recorded data was unfortunately corrupted and unusable. As a result, velocity was then determined from a previously collected dataset relating turbine power (in %) to flow velocities measured by a Nortek Vector in the same tank without any changes to the setup (*see* Supporting Information Fig. S1).

Duplicates of each optode type were used, so a total of eight optodes were used in this experiment. All optodes sampled at 1 Hz, except for the PYRO-PICO, which sampled at approximately 4 Hz on account of the sensor's fast response time. For all optodes, except the PYRO-PICO, power was supplied using an external power supply. These data were transmitted via RS232 serial communication connectors. For the PYRO-PICO, a custom data logger was built to program and acquire data from the optode via the PyroScience UART protocol. The data logger, which was controlled primarily by a SparkFun Thing Plus SAMD51 microcontroller and programmed in CircuitPython, transmitted the data via USB. The data logger and sensors were incorporated in a Blue Robotics watertight enclosure, as the PICO-O2-SUB is not a stand-alone waterproof device. The PICO-O2-SUB consists of the Pico-O2 OEM, which is enclosed in the housing with the custom data logger, and an optical feed-through SUB connector, which threads through the housing cap, that connects to the OXCAP-SUB sensor cap on the waterside of the enclosure. Data acquisition from all optodes was done centrally on a laptop using Node-RED, which is a browser-based flow editor. All data were synchronized and time-stamped in Unix time based on the laptop's clock.

The sensor response times were tested at cool and warm temperatures (~ 8°C and 16°C, respectively) in the test tank over six different flow speeds, ranging between 5 and 25 cm s$^{-1}$, with replicate runs performed at a minimum of three flow speeds for each temperature.

The flume tank did not have any temperature control. For the warm temperature experiments, the water in the flume was allowed to equilibrate to room temperature for a few days prior to the experiments. For the cool temperature experiments, the tank was emptied and refilled with water from the Arm. The exact temperature of the tank was monitored, and the tank was periodically partially drained, refilled, and mixed to keep the temperature for these experiments within 8 ± 1°C.

The response time symmetry was evaluated only at the warmer temperature, using both a step-up (undersaturated to saturated) and step-down (oversaturated to saturated) step changes in oxygen saturation. For all other experiments, the response time was evaluated using a step-up step change.

All sensors were tested together by attaching them to a support structure shown in Fig. 2b. The support structure was designed so that it could be mounted in the tank, using brackets connected to the sides of the tank. Sensors were positioned on the support structure so that all sensor faces were aligned, but without creating flow distortion for the other sensors.

The sensors were allowed to equilibrate for 10–15 min in a temperature-controlled calibration tank in Fig. 2c, d that was filled with the same source water as the flume tank. Operated by the CERC.Ocean Laboratory at Dalhousie University, this gas calibration setup (bench) allows for an automated multi-point calibration of up to eight optodes in a range of user-defined water oxygen saturation and temperature levels. For this study, the conditions were set to a fixed degree of undersaturation (~ 70%) or oversaturation (~ 125%), depending on the experiment, and maintained by the calibration bench program by controlling the flow of oxygen and nitrogen gases. The gases are then mixed and diffused into the water tank open to the atmosphere. The temperature of the bath, which controls temperature in the jacketed water tank, was set to match the temperature of the water in the flume.

After equilibration, customized sensor caps were placed on the sensors to preserve the degree of under/oversaturation of the calibration tank, as the sensors were transferred to the flume tank. The flume tank and the calibration bench were placed next to each other to ensure the quickest possible transfer of the optodes to the flume tank. Once in the flume, the caps were swiftly removed all at once by pulling on a single string that connected all caps to initiate a step change in oxygen saturation. Sensors were then allowed to equilibrate for another 10–15 min.

The optode response to a change in temperature, so-called thermal mass, at constant saturation was also evaluated. In this case, both the calibration tank and the flume were at 100% oxygen saturation. The flume was kept at room temperature (~ 16°C) and the calibration bath was kept at a cold temperature (~ 6°C). Caps were not used during this experiment, as the oxygen saturation was assumed to be constant. Additionally, in a separate experiment, the PSt3 foils were swapped between an Aanderaa 4330 and RBR*coda* T.ODO|slow to assess if the foils were indeed the same and to investigate the effect of sensor geometry on the sensor response. The response time of these swapped foil optodes was assessed over the range of flow speeds at the cool temperature (~ 8°C).

### Lab-bench response time characterization

The response time of the suite of optodes could only be evaluated over two temperatures in the flume, as the flume

has no temperature regulation. To evaluate whether or not the temperature dependence from the flume dataset could accurately be extrapolated, a lab-bench response time experimental setup was designed to evaluate the response time of an Aanderaa 4831 optode, which is the same as the Aanderaa 4330 just with a different connector, over a range of temperatures from 5°C to 30°C with a 15°C step at a range of flow speeds. Triplicate measurements were made at each temperature at a fixed flow speed estimated to be 17 cm $s^{-1}$.

The lab-bench setup in Fig. 3 consisted of two water baths and a flowthrough housing. The first water bath was an insulated temperature-controlled tank, and the second was a smaller plastic container stacked inside a larger one. Water from the temperature-controlled tank was pumped into and out of the space between the two stacked containers to make the temperature of the water inside the smaller container the same as that in the tank.

The flowthrough housing consisted of a 2-inch diameter Tee Polyvinyl chloride (PVC) fitting with the Aanderaa 4831 optode attached to an end cap that had a sub-connector bulkhead connector. This end cap was placed at one of the "long" ends of the Tee PVC fitting such that it was centered facing the "stem" of the Tee, as illustrated in Fig. 3. End caps with ¾-inch hose barbs were fixed at the other ends of the PVC fitting. The PVC fitting was oriented so water could flow along the "long" end of the Tee and exit out the "stem" at the top. This orientation was chosen to try to minimize the presence of bubbles. The flowthrough housing was connected to the tank and the small container with ¾-inch plastic tubing and a Y-valve, so water from the tank or the small container could be pumped into the housing.

For a given temperature, the tank was allowed to equilibrate with the atmosphere so that the oxygen saturation was 100%. When the small container reached the temperature of the tank, the water in the small container was bubbled with nitrogen gas until the reference optode placed in this tank was near 0% saturation and stable. When the system equilibrated, the 100% saturated water was pumped through the housing for 5–10 min until the Aanderaa 4831 readings were stable. To create a step change, the tank-side Y-valve was closed and the container-side Y-valve was opened, so 0% oxygen water was flowing through the housing. Data was collected for approximately 10 min. The volumetric flow rate was measured by manually timing the collection of outflow.

### Response time quantification

The response time was quantified by assuming the optode has a first-order exponential response to a step-change, which previous studies have shown is valid (Bittig et al. 2014) (Eq. 1).

$$y = A \times \left(1 - e^{-\frac{t-t_0}{\tau}}\right) + y_0 \quad (1)$$

where $A$ is the amplitude of the response, $t_0$ is the time the step change was initiated, $\tau$ is the 63% time constant, and $y_0$ is the offset or the initial sensor value prior to the step change. For the purpose of this paper, sensor's response time is defined as $\tau$–the 63% time constant.

The response time was determined by fitting both the optode phase measurements and oxygen saturation/concentration. Using the phase, which is the raw sensor measurement, best captures the inherent response time of the foil, while oxygen saturation/concentration depends on other sensor measurements, such as temperature from a thermistor, that have their own response time that could contaminate the optode response. But, in some practical applications, such as using BGC-Argo data, only oxygen saturation/concentration measurements are sufficiently available for response time

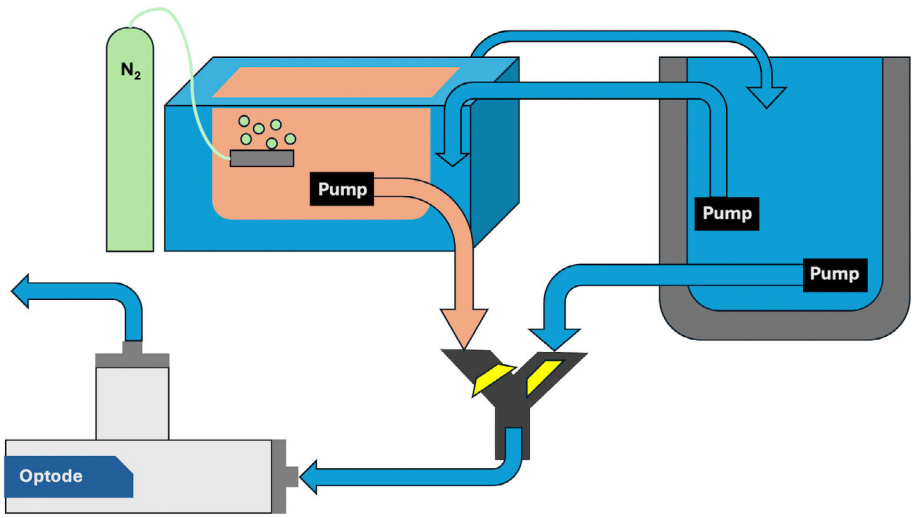


**Fig. 3.** Schematic of the lab-bench response time experimental setup. Light blue is 100% oxygen-saturated water. Light orange is near 0% oxygen-saturated water, which is achieved by bubbling nitrogen gas. Schematic is not to scale.

corrections to end users, as not all the calibration coefficients are consistently available to recalculate these values from phase measurements.

Ultimately, the response time determined from phase is different and faster than the response time determined from oxygen saturation/concentration (*see* Supporting Information Fig. S3). As a result, the response time was determined for both phase and oxygen saturation/concentration, and results will be made available for both methods. However, for this paper, only results determining the response time from oxygen concentration, with the exception of the PyroScience PICO-O2, will be shown, as this makes comparison with previous studies easier. For the PyroScience, phase was used, as all the equations and equation coefficients to convert phase to oxygen units were unknown.

The value of $t_0$ was determined manually from visual inspection of the time series, and then the sensor data were fit to Eq. 1 using scipy's curve_fit and the Levenberg–Marquardt optimization algorithm to determine the values of $A$ and $y_0$. These values of $A$ and $y_0$ were then used to normalize the data. The normalized data were fit to the linearized and normalized Eq. 1 (*see* Eq. 2) using statsmodels' ordinary least squares regression to determine the response time, $\tau$, from the slope.

$$\ln(1 - y_{\text{norm}}) = -\frac{1}{\tau}t \tag{2}$$

where $y_{\text{norm}}$ is the normalized sensor response.

The ordinary least squares fit was done excluding the first 20% and the last 15% of sensor response, that is, where $0.2 \leq y_{\text{norm}} \leq 0.85$, shown as the shaded gray region in Fig. 4. The fitting window shifts depending on the response time, so, in time units, this corresponds to $\sim 0.2\tau - 1.90\tau$. This range was chosen to reduce the fit sensitivity to the beginning of the time series, which exhibited flow disturbance from the cap removal.

### Data quality control

The flume response time data underwent a two-step quality control procedure, as preliminary analysis revealed clear outliers within the dataset. The first step was flagging data from trials that had noted errors, such as the cap was not properly removed, the optode moved out of the structure, or the optode had clearly irregular response shapes, such as those with leaking caps or bubbles on the sensor interface. The second step was flagging statistical outliers. It was assumed that the response time was linearly proportional to the inverse of flow speed at a fixed temperature, as this was found experimentally in (Bittig et al. 2014). The response time for each optode type at a given temperature was linearly fit based on this assumption. Data points that fell outside the 95% confidence intervals were flagged. All data that were flagged were not included in further analysis, resulting in approximately 50 good response times for each optode type (*see* Supporting Information Fig. S4).

### Empirical response time relationship

Previous studies used a two-layer stagnant diffusion model to determine response time based on a stagnant boundary layer thickness and temperature (Bittig et al. 2014; Bittig and Körtzinger 2017). However, while this model was used to correct BGC-Argo float oxygen profiles in the field, there are some caveats and limitations to this method. First, it requires that a velocity-boundary layer relationship is determined for each desired application, and therefore, it cannot easily be applied to new platforms. Second, it assumes that this boundary layer

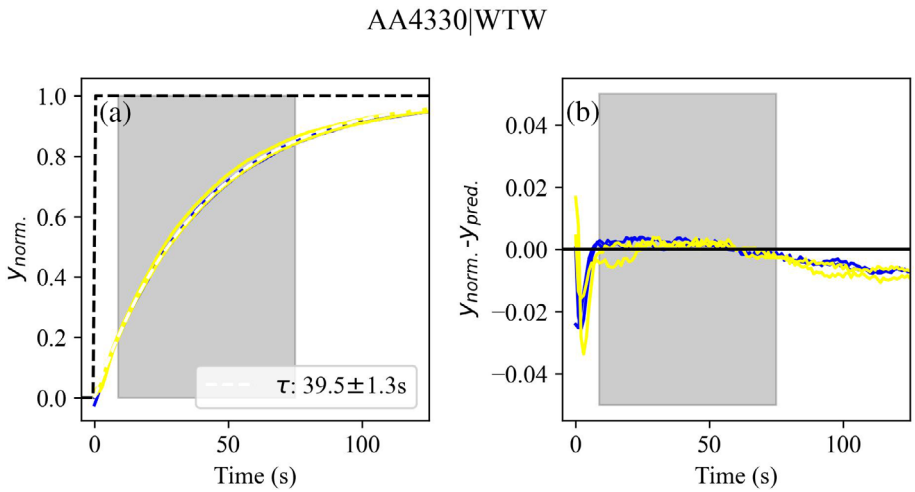


**Figure 4.** (**a**) Normalized response, $y_{\text{norm}}$, for an Aanderaa 4330W (AA4330|WTW) for four dunks (2 step down [yellow], 2 step up [blue]) at room temperature ($\sim$16°C) at the same flow speed ($\sim$25 cm s$^{-1}$) with $y_{\text{norm}}$ calculated using the mean response time from these four dunks (white dashed line). Shaded gray region is the mean linear fit regime, and the black dashed line is the idealized response. (**b**) Error of the linear defined as the difference between normalized response and predicted response, $y_{\text{pred}}$.

depends only on velocity, orientation, etc. and is independent of temperature. However, based on fluid mechanics, this assumption is invalid, and it was not consistent with results observed in the flume for the same Aanderaa 4330 optode, because Fig. 5b shows a temperature-dependent boundary layer when inferring the boundary layer thickness from the temperature and response time. As a result, an empirical formula based on a Reynolds-like number is proposed.

In fluid transport, there is the transport of momentum, heat, and mass, and each property has its own respective boundary layers (e.g., hydrodynamic, thermal, and mass concentration) that can be explicitly solved for or approximated based on the properties, both temperature dependent and independent, and the geometry of the system (Schlichting and Gersten 2017; Welty et al. 2014). For example, for laminar flow over a flat plate, the Blasius solution yields a hydrodynamic boundary layer thickness that scales with the local Reynolds number:

$$\frac{\delta}{x}=\frac{5}{\sqrt{\frac{\nu x}{\upsilon}}}=\frac{5}{\sqrt{Re_x}} \tag{3}$$

where $\delta$ is the hydrodynamic boundary layer thickness, $x$ is the distance from the leading edge of the plate, $\nu$ is the flow rate infinitely far away from the surface of the plate, $\upsilon$ is the kinematic viscosity of the fluid, which is a function of both temperature and salinity, and $Re_x$ is the local Reynolds number.

While an optode is more of a wedge than a flat plate, perhaps making the Falkner-Skan solution more appropriate, Eq. 3 can still be used as a scaling argument to estimate how characteristic diffusion time scales with properties of the flow, assuming that diffusion across the mass concentration boundary layer is the dominant control on the response time (*see* Eq. 4) (Schlichting and Gersten 2017):

$$\tau=\frac{\delta^2}{D}\sim\frac{1}{Re_x}\sim\frac{\upsilon}{\nu} \tag{4}$$

As a result, this study proposes an empirical formula (*see* Eq. 5) based on this scaling argument. This form preserves the inversely proportional relationship between response time and flow speed at a fixed temperature and the inversely proportional relationship between response time and temperature at a fixed flow speed:

$$\tau=\frac{F}{\frac{\nu}{\upsilon}+b_\nu} \tag{5}$$

where $F$ is a foil-dependent parameter, and $b_\nu$ is a flow-speed-dependent parameter. While the distance from the leading edge of boundary layer development, $x$, is unknown, it is assumed to be constant for each optode type, and it therefore becomes included in the values of $F$ and $b_\nu$.

This empirical formula has only two free parameters. The parameter $b_\nu$ was included so the response time approaches a finite limit of $F/b_\nu$ as the flow speed approaches zero. However, as the flow speed approaches infinity, meaning diffusion across the foil is the only process controlling the response time, the response time approaches zero. While diffusion across the foil is not instantaneous, it is fast compared to the measured response time over practical flow speeds, which is exemplified in both this and the previous studies (Bittig et al. 2014). Furthermore, as the application of this formula is for a range of slower flow speeds, the zero response time limit at infinite flow speed is acceptable.

## Response time corrections

If the response time is known, the optode time series can be corrected for the measurement lag, following the previously outlined methods of (Bittig et al. 2014; Gordon et al. 2020) (*see* Eq. 6)

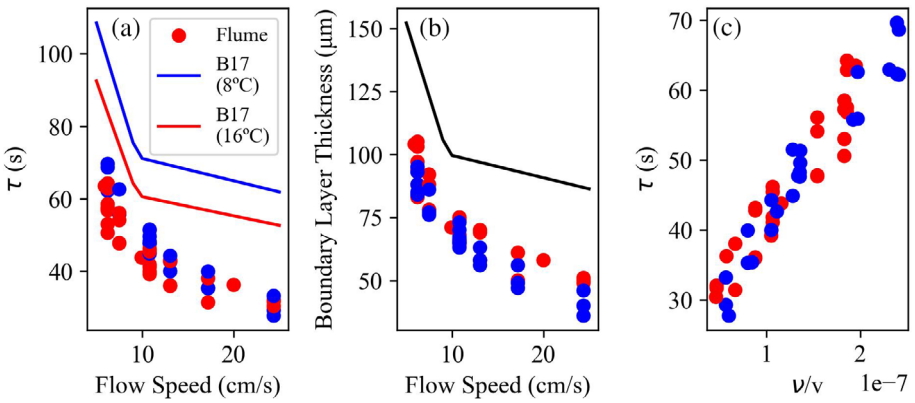


**Fig. 5.** (**a**) Response times, $\tau$, for the Aanderaa 4330 (AA4330) optodes from the flume experiments (circles) compared to those predicted by the two-layer model for a profiling float at the same flow speeds and temperatures (lines). (**b**) Boundary layer thickness predicted from the float velocity–boundary layer relationship (Bittig and Körtzinger 2017) (line) compared to inferring the thickness from the two-layer model table using the flume response times and temperature (circles). (c) $\tau$ plotted vs. the ratio of viscosity, $\upsilon$, to velocity, $\nu$.

$$\frac{c^{corr.}(t_{i+1})+c^{corr.}(t_i)}{2}=\frac{1}{2b}\left(c^{obs}(t_{i+1})-a\cdot c^{obs}(t_i)\right) \quad (6)$$

where $c^{corr.}$ is the corrected optode time series, $c^{obs}$ is the observed optode time series, and $a$ and $b$ are coefficients described by Eqs. 7 and 8.

$$a=1-2b \quad (7)$$

$$b=\left(1+2\frac{\tau}{t_{i+1}-t_i}\right)^{-1} \quad (8)$$

This method, which requires no initial conditions, is a mean filter correction, and the correction from the mean time can be linearly interpolated back to the original measurement time step.

To evaluate the performance of response time corrections in the field, profiling floats equipped with Aanderaa 4330 optodes that have reference oxygen profiles from previous studies were used. In (Bittig and Körtzinger 2017), two BGC-Argo Navis floats (WMO 690089 and 690090) equipped with both an Aanderaa 4330 and a SBE63 optodes were used. As the response time of the SBE63 was previously characterized in (Bittig et al. 2014; Bittig and Körtzinger 2017), the SBE63 oxygen profiles were response time corrected using the response times from the look-up table and pumped flow-speed-boundary layer thickness relationship (eq. A4 from Bittig and Körtzinger 2017, with $\dot{V}=600\,\mathrm{mL\,min^{-1}}$) and Eq. 6. The response time corrected SBE63 profiles were taken as the reference oxygen profiles. In (Gordon et al. 2020), 10 ElectroMagnetic-Autonomous Profiling EXplorer (EM-APEX) floats equipped with an Aanderaa 4330 optode rapidly profiled, measuring both the upcast and the downcast. Profiles were response time corrected using the response time that minimized the error between the upcasts and downcasts. These profiles, provided in the paper's published dataset, were taken as the reference oxygen profiles.

The raw Aanderaa 4330 optodes were taken as the observed time series ($c^{obs}$) and were response time corrected using Eq. 6 to obtain a corrected optode time series ($c^{corr.}$). This correction was done using the response times from both the empirical response time function from this study (Park) and the two-layer model look-up table (B17) (Bittig and Körtzinger 2017). The root-mean-squared error (RMSE) and mean absolute error between the reference oxygen profiles and the response time corrected Aanderaa 4330 profiles from Bittig and Körtzinger (2017) and gain-corrected Aanderaa 4330 profiles (Gordon et al. 2020) were calculated.

## Assessment

### Flume response time characterization

Figure 4 highlights how the flume experiments proved to be a robust way to evaluate response times as the standard deviation was low (~ 1–3 s) between replicate trials for individual sensors (*see* Table 2). Additionally, for each optode type, the computed response time for the two assets of that type had a low standard deviation across all trials, with the exception of the AA4330|WTW (*see* Table 2). For the AA4330|WTW, both assets agreed well at 16°C but not at 8°C, as one asset showed a temperature-dependent response time behavior, while the other did not (*see* Supporting Information Fig. S5). It is not clear why this was the case.

**Table 2.** Mean standard deviation of the response times (in seconds) from flume replicates for individual optodes (Asset 1 and 2) and between two assets for each optode type (1 + 2).

| | Mean standard deviation of response times (s) | | | |
|---|---|---|---|---|
| | AA4330\|WTW | AA4330 | RBR\|SLOW | PYRO-PICO |
| Asset 1 | 1.8 | 0.80 | 1.3 | 0.42 |
| Asset 2 | 3.5 | 1.1 | 0.59 | 0.48 |
| 1 + 2 | 5.0 | 2.7 | 1.6 | 0.34 |

Additionally, as the $R^2$ and RMSEs in Table 3 show the assumption that the optode has a first-order exponential response to a step change was valid, and the proposed exponential function fit well. Furthermore, the assumption of a single time constant can be assessed by comparing the time it takes for the sensor to reach 90% ($t_{90}$) or 95% ($t_{95}$) to 63% ($t_{63}$) of its normalized response. If the optode truly has a first-order exponential response with one time constant, $\tau$, the ratios of these values should be 2.3 and 3.0, respectively. From these ratios of time constants in Table 3, it appears that the RBR|SLOW may have a slower, secondary response, but all other optodes types exhibit a first-order exponential response.

An important caveat noted after data collection was the fact that the cap removal process did appear to temporarily cause flow disturbance, which artificially increased the turbulence at the sensor's foil and temporarily reduced the response time. However, the restoration of normal flow was observed after this disturbance, and fitting the response time over 20–85% of the sensors' response allowed a consistent response time, as exemplified in Fig. 4 and Table 2, to be determined.

All optode types showed a symmetric response at room temperature, meaning the response time was the same for both an increase and decrease in oxygen saturation, as illustrated in Fig. 4 with duplicate step up and down dunks at the 25 cm $s^{-1}$ and 16°C (*see* Supporting Information Fig. S6 for results from other optodes). Figure 6 shows that all optodes in this study have an inverse relationship between response time and both flow speed and temperature. These results are consistent with previous studies, as higher flow speeds result in thinner fluid boundary layers and, therefore, a larger oxygen gradient immediately at the sensor interface, while higher temperatures result in higher rates of diffusion of oxygen to the sensor interface (Bittig et al. 2014).

**Table 3.** Median values of different metrics for response time fits. $R^2$ is the $R^2$ values (unitless) from the ordinary least squares fit. The root-mean-squared error (RMSE) is using the final values of $A$, $\tau$, and $b$ (units: $\mu$mol kg$^{-1}$, except for PYRO-PICO which is in degrees). $t_{90}/t_{63}$ and $t_{95}/t_{63}$ is the ratio of the time it takes the sensor to reach 90%, $t_{90}$, and 95%, $t_{95}$, of its response to the time it takes the sensor to reach 63% of its response, $t_{63}$, respectively. If the response is an ideal, first-order exponential response, the $t_{90}/t_{63} = 2.3$ and $t_{95}/t_{63} = 3.0$.

| | Median fit values | | | |
|---|---|---|---|---|
| | **AA4330\|WTW** | **AA4330** | **RBR\|SLOW** | **PYRO-PICO** |
| $R^2$ | 1.00 | 1.00 | 0.999 | 0.997 |
| RMSE ($\mu$mol kg$^{-1}$) | 0.32 | 0.39 | 0.59 | 0.0087° |
| $t_{90}/t_{63}$ | 2.31 | 2.31 | 2.4 | 2.3 |
| $t_{95}/t_{63}$ | 3.04 | 3.07 | 3.25 | 3.1 |

The optodes tested had a wide range of response times, summarized in Table 1 and shown in Fig. 6, with the following ranking from fastest to slowest: PYRO-PICO, RBR|SLOW, AA4330, AA4330|WTW. The PYRO-PICO and RBR|SLOW response times are consistent with the manufacturer reported response time of < 3 s and < 30 s, respectively. However, for both the AA4330 and AA4330|WTW, the measured response times are greater than the manufacturer reported response times over the range of flow speeds tested (*see* Table 1).

### Lab-bench response time characterization

The goal of these experiments was to determine the response time of an Aanderaa optode across a range of oceanographically relevant temperatures at different flow speeds. However, while conducting these experiments, it became clear that the measured response times were faster than expected when calculating flow speed from the volumetric flow rate and cross-sectional area of the pipe. As a result, these data could not be directly compared to the results from the flume. However, they could be used to better understand and assess the strengths and limitations of testing setups on response time.

The lab-bench experiment utilized a blind tee, where the fluid entering the system is forced to bend and leave through

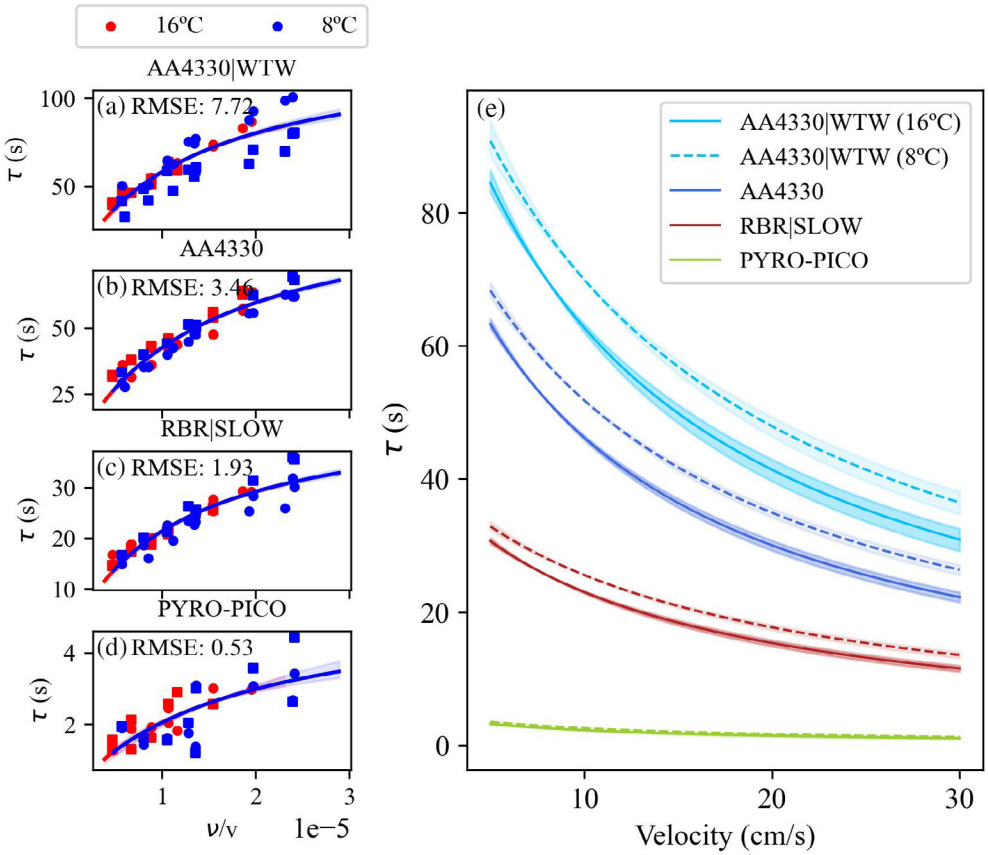


**Fig. 6.** (**a**–**d**) Response time, $\tau$, by optode sensor type vs. the ratio of viscosity, $\upsilon$, to velocity, $v$, at 16°C (red) and 8°C (blue). Marker shape (circle, square) denote individual sensors. Solid lines are the empirical fit with the reported fit RMSE in seconds. Shaded region is plus/minus one standard deviation of the fit parameters. (**e**) Response time, $\tau$, empirical fits by optode sensor type vs. inverse flow speed. Line style indicates temperature (solid: 16°C, dashed: 8°C). Shaded region is plus/minus one standard deviation of the fit parameters.

an outlet perpendicular to the inlet flow, illustrated in Fig. 3. This setup results in fluid dynamics that are different from both the flume and a profiling float, where the flow is not necessarily along the same axis that the sensor is oriented. In a blind tee, there is a pressure drop around the inside of the bend, causing the flow to accelerate, and on the outside of the bend, there is an adverse pressure gradient, causing the flow to decelerate (Han et al. 2022). This results in a shifting of the maximum velocity off the centerline, causing the flow to split, sending some flow to recirculate in the blind tee. A number of computational fluid dynamic studies have modeled the flow in a blind tee configuration to analyze mixing within the blind tee (Han et al. 2022, 2024; Lan et al. 2022). While these simulations do not analyze flow with an object in this system, the results show how the flow speed varies within the region where the sensor was located. Additionally, the fluid flow was not fully developed in these experiments as the sensor position from the inlet was much less than the hydrodynamic entrance length. These two factors likely contribute to why the speed dependence of the lab-bench response experiments could not be compared with the flume-based results.

While this setup could not be used to replicate comparable results to those observed in the flume, it could, however, be used to assess the optode's fastest response time. While most of the response times were determined at flow rates less than 2.5 L $min^{-1}$, data were collected at higher flow rates, resulting in response times ranging from 11 to 14 s. Figure 7 shows the minimum response time for the Aanderaa 4831, or more specifically the Pst3 foil used in both the Aanderaa 4330 and 4831, determined by fitting these data to the inverse of volumetric flow rate, and is estimated to be 8 s. For the same optode tested in a flow-through setup (Bittig et al. 2014) found minimum response times ranging from 4 to 8 s. If stronger pumps were used in this setup, it is likely that these faster response times could have been achieved.

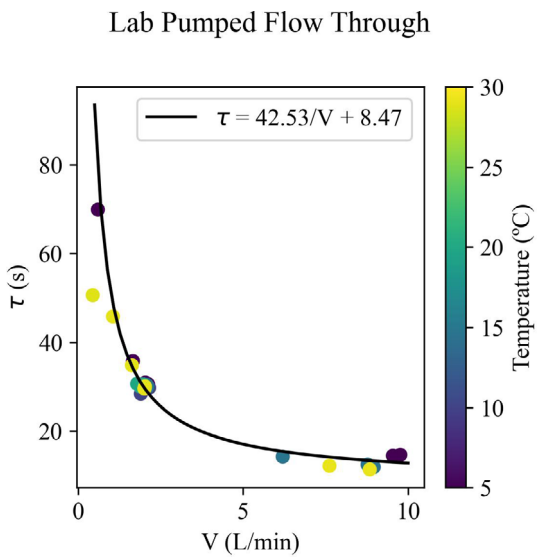


**Fig. 7.** Response time, $\tau$, for the Aanderaa 4831 vs. volumetric flow rate, $V$, color-coded with temperature.

These fast response times at high flow speeds represent the case when the boundary layer is small and diffusion of oxygen across the sensing foil is the only process affecting the response time. These results support the assumption that diffusion of oxygen across the boundary layer is the dominant process affecting the response time, as the measured response times were at least 3 times larger than the response times of this limiting case.

### Assessment of the empirical response time relationship

The empirical formula described by Eq. 5 fits the flume response time data reasonably well because the RMSEs of the fits reported in Fig. 6 were comparable to the replicate mean standard deviations in Table 2. Using the ratio of viscosity to flow speed as the predictor overall did a good job of capturing both the flow speed and temperature dependence of the response time. What is particularly interesting is that the temperature dependence of viscosity seems to explain the temperature dependence of the response time perfectly across all optode types, as the warm and cold response times are indistinguishable in Figs. 5c and 6a–d. What this likely means is that the temperature dependence of the boundary layer thickness controls the response time instead of the temperature dependence of diffusion of oxygen in both the boundary layer and foil.

While the response times from this study's lab experiments could not be used to evaluate the performance of the formula over a wider range of temperatures, the predicted response times from this formula for the AA4330 were compared to those determined from experiments 1–4 from Bittig et al. (2014), which spanned from ~0°C to 30°C, and there was good agreement (RMSE: 4.9 s, *see* Supporting Information Fig. S7).

The benefit of this empirical formula is that it allows for not only the response time to quickly be calculated from temperature, salinity (as both determine viscosity), and velocity, but also for an easy comparison of response time behaviors between optode types. However, because this is an empirical formula, the exact meaning of each fit parameter in Eq. 5 does not clearly link to a physical quality or process. However, based on the values of the fit parameters $F$ and $b_v$ reported in Fig. 8, it appears that perhaps $F$ is related to the foil properties or sensor response time, and $b_v$ is related to the flow speed and geometry dependence of the response time.

The value of $F$ is related to the magnitude of the response time and seems to reflect the inherent response time characteristics of the foil. The ranked values of $F$ from highest to lowest in Fig. 8 correspond with the ranked optode response times from slowest to fastest. Therefore, it is believed that the larger the value of $F$, the slower the response time.

Mathematically, the value of $b_v$ determines the linearity or nonlinearity of the flow speed dependence at a fixed

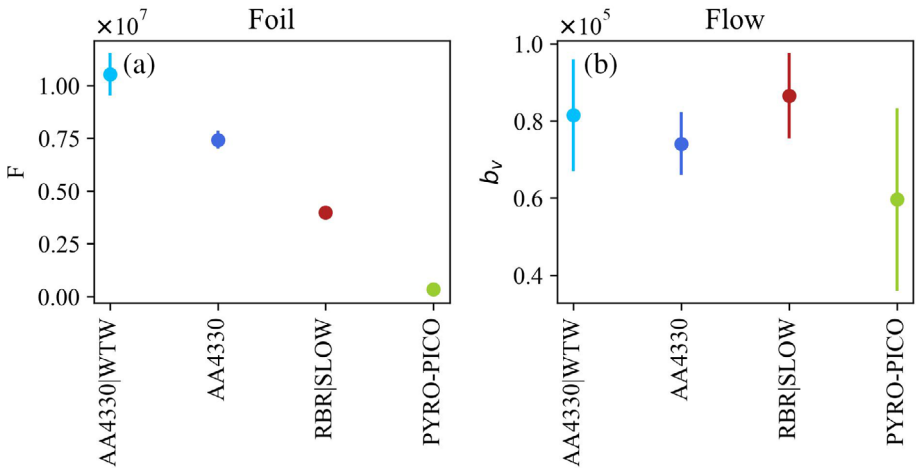


**Fig. 8.** Fit parameters (**a**) $F$ and (**b**) $b_v$ from Eq. 5 for each optode type. Error bars are one standard error of the fit parameters.

temperature (*see* Eq. 5). When $b_v$ equals 0, the flow speed dependence is perfectly linear. Figure 8 shows that the PICO-O2 has the most linear flow speed dependence, while the RBR|SLOW has the most nonlinear flow speed dependence. The value of $b_v$ may potentially be related to the sensor geometry, as the two Aanderaa optodes have nearly identical $b_v$ values. However, it is important to recall that $b_v$ was included in this form to have a finite response in the limit as flow speed goes towards zero. Furthermore, these values, demonstrated by overlapping error bars in Fig. 8, are not statistically significantly different, so these interpretations are only speculative.

These empirical formulas were then applied to a range of oceanographic temperatures and profiling speeds to recreate the response time contours, similar to those provided in (Bittig et al. 2014; Bittig and Körtzinger 2017) for a profiling float in Fig. 9. These contours are smooth with a finite limit as flow speed approaches zero.

### Evaluating response time on BGC-Argo floats

To assess the performance of estimating the response time in the field, the predicted response times from this study were used to correct oxygen profiles from a total of 12 different profiling floats equipped with the AA4330 optodes listed in Table 4. These results were compared to the reference oxygen profiles for each float. There were no other data sets available to assess the field performance of this empirical formula for the other optode types (AA4330|WTW, RBR|SLOW, PYRO-PICO).

For the two BGC-Argo profiling floats (WMO 6900889 and 6900890), the reference oxygen profile was the response time corrected SBE63 optode (Bittig and Körtzinger 2017). These floats profiled at approximately 10 cm $s^{-1}$. As shown in Fig. 10c, g and summarized in Table 4, the response times predicted by this study for these floats (~ 50 s) were faster than those predicted by the two-layer model (~ 70 s). The two-layer model response times reportedly did a better job correcting the AA4330 profile to match the SBE63 oxygen profiles, as the calculated RMSEs and mean absolute error were lower using these values.

For the 10 other profiling floats, the reference oxygen profile was the response time corrected profile found by minimizing the errors between the upcast and downcast profiles

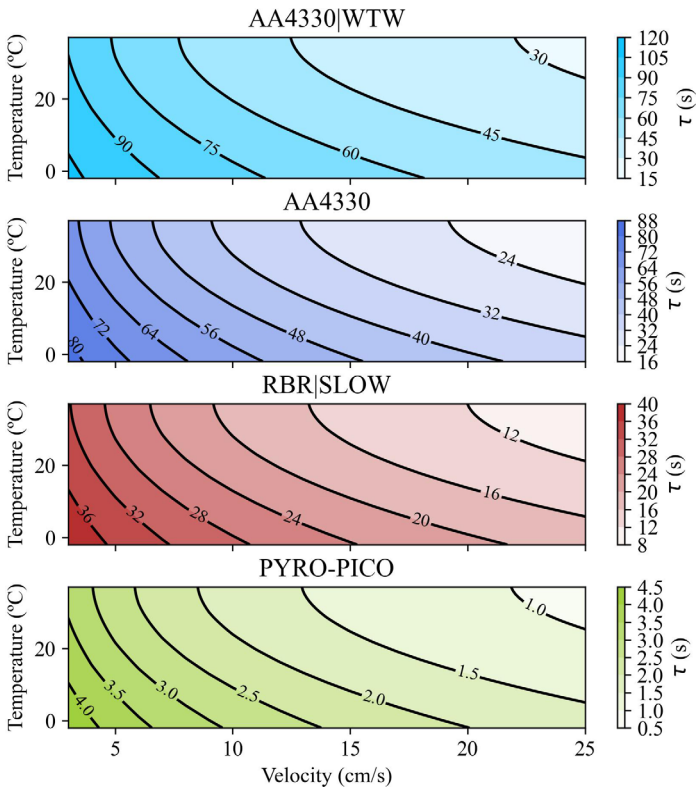


**Fig. 9.** Response time, $\tau$, as a function of temperature and flow speed for four different optode types: Aanderaa 4330W (AA4330|WTW), Aanderaa 4330, and RBR*coda* T.ODO|slow (RBR|SLOW), and PyroScience PICO-O2-SUB (PYRO-PICO). Temperatures range from −2°C to 38°C, and velocities range from 3 to 25 cm $s^{-1}$ with salinity = 35.

**Table 4.** Response time correction statistics for 12 profiling floats. The median response time, $\tau$, and standard deviation, $\sigma$, for all float profiles using this study's (Park) and the Bittig response times. The median root-mean-squared error (RMSE) and mean absolute error (MAE) was also calculated between the time-lagged reference oxygen profile and the observed Aanderaa 4330 optode profiles. Shaded cells indicate where using Bittig response times resulted in the same or better performance statistics compared to this using this study's response times.

| | Park | | | | Bittig | | | |
|---|---|---|---|---|---|---|---|---|
| | $\tau$ (s) | $\sigma$ (s) | RMSE ($\mu$mol kg$^{-1}$) | MAE ($\mu$mol kg$^{-1}$) | $\tau$ (s) | $\sigma$ (s) | RMSE ($\mu$mol kg$^{-1}$) | MAE ($\mu$mol kg$^{-1}$) |
| 6900889 | 52 | 6.1 | 4.34 | 1.91 | 71.1 | 8.5 | 4.04 | 1.64 |
| 6900890 | 52.1 | 6.5 | 3.47 | 2.13 | 71.4 | 8.8 | 2.75 | 1.85 |
| f7939 | 41.1 | 3.9 | 1.42 | 0.85 | 67.3 | 6.9 | 0.7 | 0.4 |
| f7940 | 45.9 | 3.8 | 1.23 | 0.61 | 69.2 | 7.2 | 0.5 | 0.23 |
| f7941 | 45.3 | 4.3 | 1.27 | 0.65 | 67.9 | 7.4 | 0.54 | 0.26 |
| f7942 | 43.9 | 4.9 | 1.3 | 0.72 | 67.1 | 7.4 | 0.56 | 0.29 |
| f7943 | 45.7 | 4.7 | 1.55 | 0.82 | 68.5 | 7.5 | 0.8 | 0.41 |
| f7944 | 46.3 | 3.9 | 1.32 | 0.7 | 69.3 | 7.3 | 0.63 | 0.32 |
| f7945 | 49.2 | 22.6 | 0.99 | 0.48 | 72.9 | 19.4 | 0.59 | 0.31 |
| f8081 | 39 | 5 | 1.14 | 0.7 | 66.5 | 7.5 | 0.41 | 0.24 |
| f8082 | 45.5 | 3.9 | 1.4 | 0.73 | 69 | 7.3 | 0.68 | 0.34 |
| f8083 | 40.6 | 4.9 | 1.28 | 0.76 | 66.9 | 7.5 | 0.55 | 0.29 |

(Gordon et al. 2020). These floats profiled at approximately 12 cm s$^{-1}$. Again, the Bittig response times ($\sim$ 67–70 s) did a better job correcting the AA4330 profile to match the reference oxygen profiles, as shown in Fig. 10h. This is not surprising as the response time that minimized the errors between the upcast and the downcast was in good agreement to those predicted using the Bittig two-layer model (Gordon et al. 2020).

While for both independent sets of float data the Bittig two-layer model response times resulted in the best response time corrections, an important question remains unanswered: What causes this difference in response time for the same sensor at the same temperature and flow speed? This question is something that was brought up in the original studies investigating this work, but never explicitly answered (Bittig et al. 2014; Bittig and Körtzinger 2017). In the original study, response times estimated from comparing reference CTD oxygen profiles to those on profiling floats ($\sim$ 100–200 s) were much larger than those observed in lab experiments. However, upon a subsequent study using the dual-optode floats (WMO 6900889 and 6900890) to determine in situ response times, it was found that the response time was faster ($\sim$ 60–100 s), but little explanation was given for what accounts for why these response times are still slower than what was observed in lab experiments.

Here, we would like to speculate as to factors accounting for these discrepancies, as insufficient field data is currently available to validate these theories, and recommend further research to determine the best way to consistently translate results from the lab into the field.

1. Impacts of float geometry: In the flume, the optodes were aligned and the first object to disturb the surrounding flow field. However, on a float, the geometry of the float cap results in flow disturbances upstream of the optode position. The presence of the antenna and CTD could result in a wake that leads to flow separation, potentially isolating the optode from changes in the surrounding flow that would result in an apparent increase in response time. On gliders, a computational fluid dynamics study revealed that the typical optode placement behind the fin was in a laminar wake region, drastically reducing the flow speed at the sensor position (Moat et al. 2016). As a result, placing the optode on the tail facing the direction of attack was found to be better for improving the response time (Nicholson and Feen 2017).
2. Unsteady profiling velocity: While floats ascend at a relatively consistent speed, there is variation in the float velocity due to the buoyancy control (*see* Fig. 10). As a result, the float is constantly accelerating and decelerating. This process can result in changes in boundary layer and wake/flow separation, potentially resulting in an increase in response time. Accelerating flow tends to result in a thinner boundary layer, while deceleration results in a thicker one (Lautrup 2011). The flume experiments were conducted with steady flow and minimal acceleration.
3. Uncertainties with estimating response times from upcast and downcasts: In the case of (Gordon et al. 2020), response times were determined by finding the one that minimized the RMSE between the corrected up and downcasts, and these closely agreed with response times predicted by the Bittig two-layer model. This method has been used to correct for thermal lag errors on gliders (Garau et al. 2011). While gliders are more hydrodynamic and profile at an angle, floats, on the other hand, are not, making

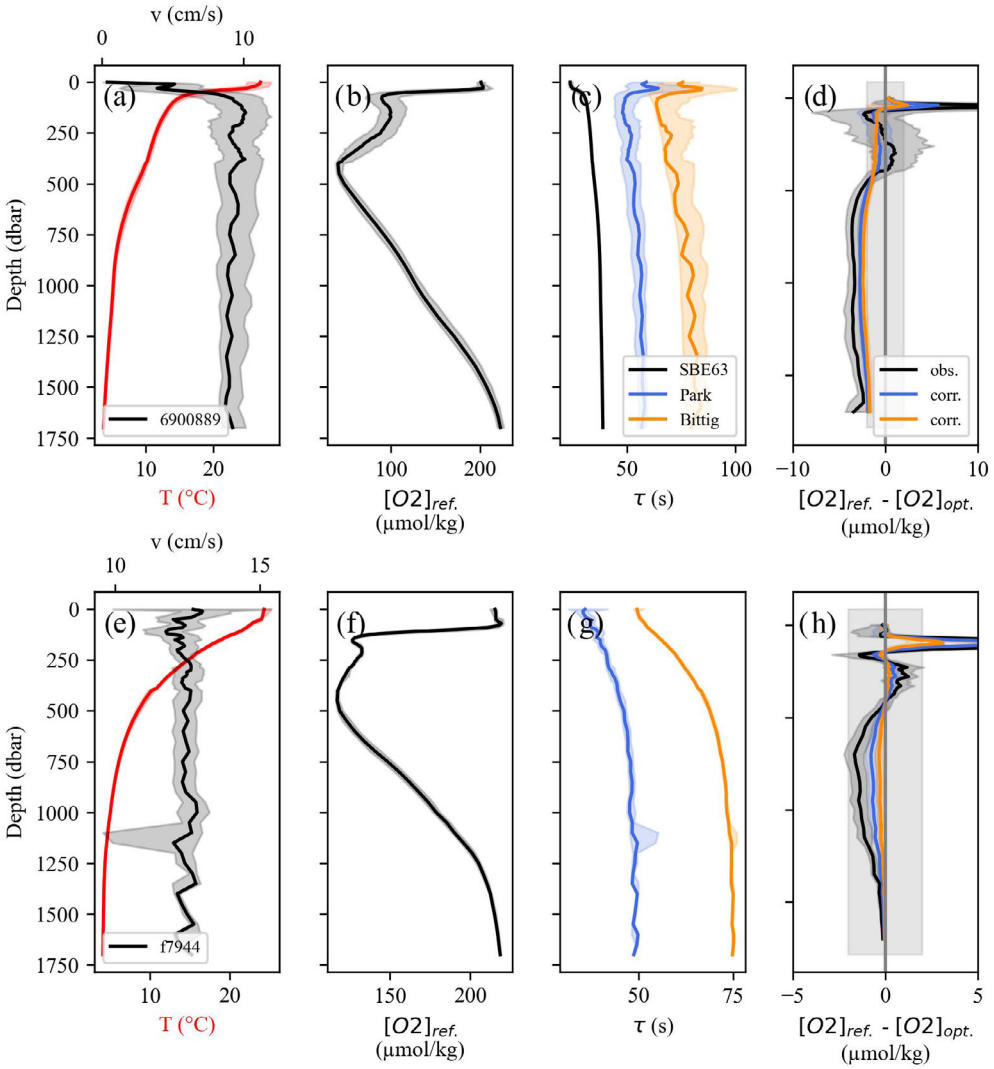


**Fig. 10.** Median profiles (solid line) with 25th/75th quantiles (shaded) for two profiling floats (**a**–**d**) WMO 6900889 from Bittig and Körtzinger (2017) and (**e**–**h**) f7944 from Gordon et al. (2020): (**a**, **e**) temperature (°C) in red and profiling velocity (cm $s^{-1}$) in black, (**b**, **f**) the reference dissolved oxygen concentration, $[O2]_{ref.}$ ($\mu$mol $kg^{-1}$), (**c**, **g**) response times, $\tau$, using this study's empirical formula (Park [blue]) and the Bittig two-layer model response time (SBE63 [black] and Bittig [orange]), (**d**, **g**) difference between $[O2]_{ref.}$ and the Aanderaa 4330, $[O2]_{opt.}$, with (corr.) and without the response time correction (obs. [black]). Vertical gray shading denotes $\pm 2\,\mu$mol $kg^{-1}$, which is approximately the accuracy of the Aanderaa 4330 optode.

the downcasts far more noisy and turbulent than the upcasts (Gordon et al. 2020). As the float body disrupts the flow first, based on the float geometry argument, this can result in an apparent slower response to environmental changes and likely an overall overestimation of the response time, like has been observed on gliders (Moat et al. 2016)

Ultimately, based on the data available, it is impossible to make a conclusive statement as to what accounts for these differences. While many floats now are built with in-air measurement capabilities, the optode position is not necessarily uniform in its location, but is consistently downstream from the initial flow disturbance (Bittig et al. 2015b). Perhaps aligning the optode with the antenna to minimize flow disturbance would lead to better agreement between lab and field response times for the same optode at the same temperature and flow speed. However, additional field studies, and perhaps computational fluid dynamic simulations, are needed to improve our understanding of this phenomenon and recommend best practices as to how to consistently address it moving forward.

### Temperature response at constant $pO_2$

One of the goals of this study was to determine how optodes respond to a change in temperature while keeping the partial pressure of oxygen constant ($pO_2$), as it is in

equilibrium with the atmosphere. A perfect sensor under these conditions should show no change in $pO_2$ and a step change in oxygen concentration, as a result of the step change in temperature and the change in oxygen solubility as demonstrated in Fig. 11. This is because diffusion of oxygen is driven by a gradient in $pO_2$, and, if there is no gradient, the sensor should have no response in oxygen saturation. However, a perfect sensor response was most closely observed with the RBR|SLOW, but not the AA4330 and AA4330|WTW (*see* Fig. 11 and Supporting Information Fig. S8).

Figure 11 shows that for the AA4330 (and also the AA4330|WTW), an initial step in temperature followed by a slow adjustment to ambient temperature was recorded by the thermistor. This behavior resulted in an initial spike in both oxygen saturation and concentration, followed by a slow ($\sim$ 25 s) adjustment to the flume environment. The RBR|SLOW showed a similar but less dramatic result (*see* Supporting Information Fig. S8). While the observed spikes in phase across all optodes in the initial $\sim$ 10 s could be due to measurement phase changes (water to air and air to water), these effects should be minimal as $pO_2$ should be constant in the bath, air, and flume, as they were all in equilibrium with the atmosphere. As a result, this interesting sensor behavior is due to the temperature effects.

There are several aspects of the sensor response that contribute to the observed behavior, the first being the thermistor response time. The thermistor response was clearly not a first-order exponential, so the thermistor response was assessed using $t_{63}$, $t_{90}$, and $t_{95}$ (*see* Fig. 11; Supporting Information Figs. S8 and S9). For both the Aanderaa and RBR optodes, the $t_{63}$ was short ($\sim$ 1 s) and in agreement with the manufacturer reported response times, < 2 s and < 1 s, respectively. However, for both Aanderaa optode types, the $t_{90}$ and $t_{95}$ for these sensors' thermistors were close to the optode response times and showed a flow speed-dependent response (*see* Supporting Information Fig. S9). The RBR thermistor was notably faster than the Aanderaa thermistors and showed minimal flow-speed dependent response. As the manufacturers report differences in response time, this is likely due to differences in thermistors.

Thermal inertia errors are those that result from differences in temperature and the variable of interest, like oxygen, response times. They have been studied and quantified for CTDs, and these studies have found that the storage of heat in the sensor walls to warm/cool the sensing area dominates these errors (Dever et al. 2022; Lueck 1990; Lueck and Picklo 1990). Ultimately, when an optode's thermistor is used to calculate oxygen saturation and concentration from phase measurements, the assumption is that the thermistor temperature is representative of the optode's foil and, therefore, measurement temperature. However, if the temperature of the foil is solved for such that it matches an ideal foil response (i.e., instantaneous change in oxygen saturation and concentration to the flume values), as is done in Fig. 11, it becomes apparent that this assumption might not be valid and that the foil has a slower temperature response than the thermistor (*see* Supporting Information Figs. S8 and S9).

These effects are most notable in both the AA4330 and AA4330|WTW, and not the RBR|SLOW. Any temperature effects from the RBR|SLOW are minimal, as the sensor has nearly ideal step response, and these effects could easily be removed through simple smoothing or spike removal. When

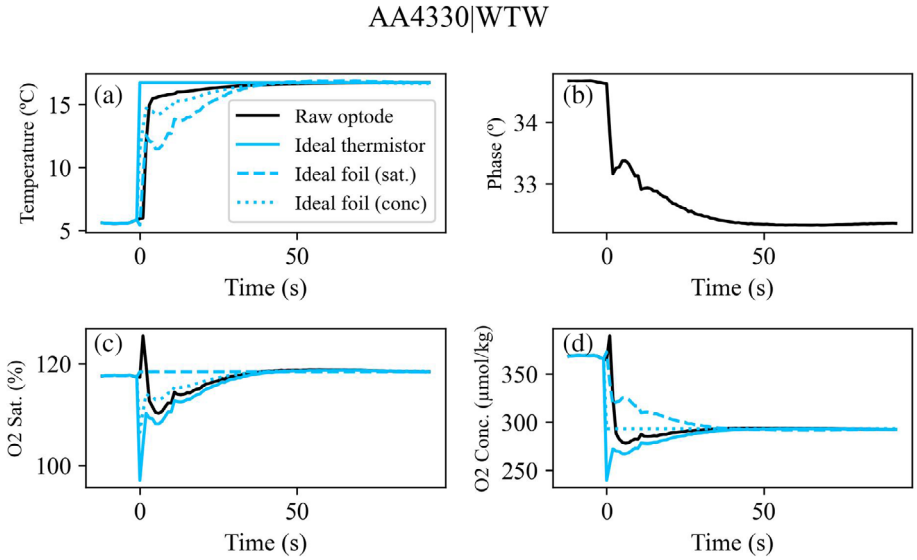


**Fig. 11.** Response of an Aanderaa 4330 W (AA4330|WTW) optode to a step change in temperature at $\sim$ 11 cm $s^{-1}$ in: (**a**) temperature, (**b**) phase, (**c**) oxygen saturation ($O_2$ Sat.), and (**d**) oxygen concentration. Black indicates the observed response. Solid colored line indicates the response using an ideal step change in temperature. Dashed and dotted colored lines indicate the response assuming an ideal foil response in oxygen saturation and concentration, respectively.

comparing the estimated $t_{90}$ and $t_{95}$ of the AA4330 and AA4330|WTW foils from Supporting Information Fig. S9, the values are comparable, suggesting that this response depends on sensor geometry and not foil type, as the difference between these two optodes is only the foil. These results are sensible because the Aanderaa has a lower surface area to volume ratio of the sensor body, which reduces heat transfer, and a larger area of exposed foil than the RBR.

These results show that the Aanderaa optodes can show significant thermal inertia errors, while the RBR|SLOW optodes do not. While this study does not provide a solution on how to address these errors, it felt important to highlight these findings for future studies.

### PSt3 foil variability

According to the manufacturers, RBR|SLOW and AA4330 supposedly use the same PSt3 foils. However, as Fig. 6e shows, the RBR|SLOW has nearly twice as fast a response compared to the AA4330, which could partially be explained by the sensor geometry. Furthermore, the AA4330 showed a nearly ideal first-order exponential response in Table 3, while the RBR|SLOW showed potential for a slower secondary response. To assess whether this was due to differences in foils, sensor geometry, or something else, the foils from one RBR|SLOW and AA4330 were swapped and the response time was assessed over a range of flow speeds at 8°C. For this analysis, the response times calculated from phase were used to avoid any impacts from the calibration coefficients and temperature-dependent effects.

Figure 12 shows that the AA4330 PSt3 foil had a similar response time in both the AA4330 and RBR|SLOW optode, suggesting that the differences in response time between the two optodes are due to differences in foils. However, the RBR|SLOW PSt3 foil in the AA4330 resulted in response times approximately twice as slow as the same foil in the RBR|SLOW optode. If these differences were solely due to differences in the foils, the expected outcome would be that the RBR|SLOW foil would have the same response time in both optode types, but it is clear there are other factors at play that are affecting the response time.

The results of this experiment do not allow for a conclusive assessment, only speculations that future studies could explore. The RBR|SLOW PSt3 foil emerges as more sensitive to the sensor geometry or mechanics causing faster response

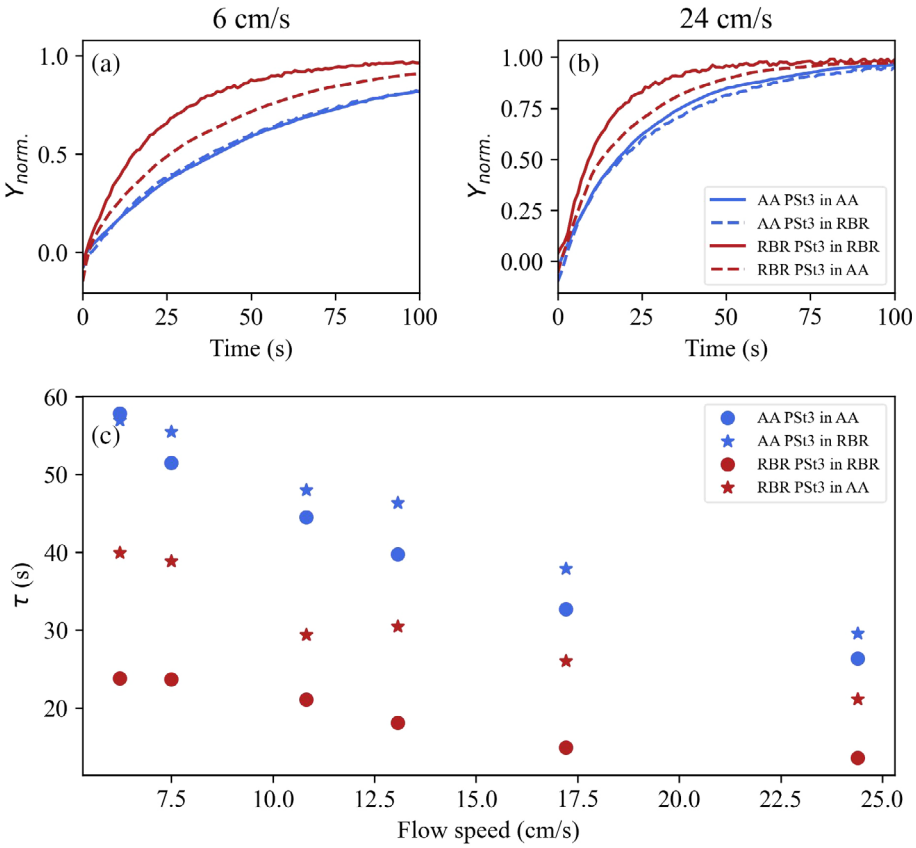


**Fig. 12.** Normalized response for the Aanderaa PSt3 foil in the Aanderaa 4330 (AA4330) optode (blue solid line, blue circle), the Aanderaa PSt3 foil in the RBR*coda* T.ODO|slow (RBR|SLOW) optode (blue dashed line), the RBR|SLOW PSt3 foil in the AA4330 optode (red dashed line), and the RBR|SLOW PSt3 foil in the RBR|SLOW optode (red solid line) at (**a**) 6 cm $s^{-1}$ and (**b**) 26 cm $s^{-1}$. (**c**) The response time, $\tau$, over a range of flow speeds (cm $s^{-1}$) where the solid lines are circles and the dashed lines are stars.

time. Sensor geometry affects the flow, and ultimately the boundary layer formation, which could perhaps be explained by differences in optode size. The AA4330 diameter is 36 mm, while the RBR|SLOW is 28 mm in diameter. The exposed foil surface area is larger on the AA4330 compared to the RBR|SLOW. While this exposed foil area should not directly affect the response time, it perhaps indicates that the AA4330 samples a larger area of foil, resulting in a longer response time.

Ultimately, it is clear that the response time of RBR|SLOW PSt3 foil is dominated by the "rate-limiting" step, which appears to be an inherent property of the foil and could be taken advantage of with the RBR|SLOW sensor geometry. On the other hand, AA4330 foil appears to be less responsive to the sensor geometry, and when paired with RBR|SLOW optode has even slightly slower response time (Fig. 12c). As this is just one experiment, additional, more comprehensive research is needed to better determine the controls of the response time of these foils. However, it is clear that the foils used by RBR|SLOW and AA4330 are not identical, despite the manufacturer's claim.

## Discussion

This study characterizes the response time of four different oxygen optodes; notably characterizing these values for most of these sensors the first time. Here it is demonstrated that the flume setup is an effective environment for testing the response time for a suite of optodes over a range of profiling flow speeds (5–25 cm $s^{-1}$) at two distinct temperatures (8°C and 16°C), as there was good agreement between replicates (demonstrated in Fig. 4 and Table 2). These methods provide an effective and consistent way to batch characterize sensor response time. Results from this study support the assumption that optodes have a first-order exponential response with one time constant (Table 3), as was proposed by (Bittig et al. 2014). Furthermore, this study highlights the importance of characterizing both the flow speed and temperature dependence of oxygen optode response times for profiling applications, because experimental response times (Fig. 6) can be much slower than manufacturer reported ones (Table 1), which can increase sources of measurement uncertainty in the field. This was most notable for the Aanderaa 4330 and 4330W, as the RBR*coda* T.ODO|slow and the PyroScience PICO-O2-SUB best agreed with the manufacturer reported response times.

In contrast to previous studies, which use a two-layer diffusion model to determine response time as a function of boundary layer thickness and temperature (Bittig et al. 2014; Bittig and Körtzinger 2017), this study leverages boundary layer theory and proposes that the response time of an optode scales with a Reynolds-number-like value (Eq. 5). This provided a consistent way to scale response times across optode types. This empirical formula is novel because it allows for the response time to be determined for a suite of optodes without having to define a velocity-boundary layer relationship for each optode type and application, if the local velocity is known. Furthermore, it revealed that the temperature dependence of viscosity explains the temperature dependence of the response times for all optode types (Figs. 5, 6), meaning that the boundary layer thickness, which scales with viscosity, controls the temperature dependence of the response time instead of rates of diffusion.

This study was consistent with previous studies, as response times determined in the lab at the same flow speed and temperature were much faster than those observed and used in the field to correct BGC-Argo oxygen profiles (Figs. 5, 10) (Bittig et al. 2014; Bittig and Körtzinger 2017; Gordon et al. 2020). As a result, this formula underperformed in comparison to the existing two-layer model for the AA4330 used to response time correct profiles on this platform (Fig. 10 and Table 4). The question still remains: What accounts for these discrepancies between lab and field response times for the same sensor at the same flow speed and temperature? This study hypothesizes that these differences are due to factors such as the impacts of float geometry on downstream flow and accelerating/decelerating flow on the boundary layer that decrease or effectively decrease the flow speed at the optode sensing foil relative to the profiling velocity of the float. However, additional field trials and perhaps computation fluid dynamics simulations are needed to better understand these processes and to recommend methods for translating laboratory results to the field in a consistent manner.

So, what are the implications of properly (or improperly) applying these response time corrections? To answer that, these response time errors need to be contextualized within the broader sources of uncertainty related to oxygen optode performance, specifically for the AA4330, on BGC-Argo floats to determine when these corrections are important. Aanderaa reports that these optodes have an accuracy of $< 2\ \mu$M, but in practice these values depend on calibration methods, such as multi-point calibrations, which have an accuracy of $\sim 1\%$ (Aanderaa Data Instruments AS n.d.). However, optodes are known to exhibit irreversible storage drift, where the accuracy of the optode decreases from the most recent calibration while it is stored prior to deployment, resulting in errors that can be on the order of $-10\%$ (Bittig et al. 2018; Bittig and Körtzinger 2015; Johnson et al. 2015; Takeshita et al. 2013). While these optodes are stable with time once deployed, they can still exhibit a drift of $\sim 1\%$ per year (Miller et al. 2024). Thankfully, on BGC-Argo floats, the storage and time drift can be corrected using in-air calibrations, which can correct the accuracy of these optodes back to 1% (Bittig and Körtzinger 2015). Additional sources of uncertainty are a reversible, pressure-dependent drift, with a magnitude of 0.85–3.3% per 1000 m, which is relevant for floats when they are idle at 1000 m for 10 d (Bittig et al. 2015a; Miller et al. 2024). To summarize, the estimated practical uncertainty

of AA4330 optodes on BGC-Argo floats ranges from ~1% to 6%, depending on measurement depth. In a review of BGC-Argo float performance in the Southern Ocean and Mediterranean, the practical accuracy, when compared to ship-based oxygen measurements, was ~1–3% (Johnson et al. 2017; Mignot et al. 2019).

The errors resulting from not response-time correcting oxygen profiles, as exemplified in Figs. 1 and 10, are comparable to those of the sensor, if the error, for simplicity, is assumed to be a constant 2 $\mu$mol kg$^{-1}$. However, in regions with a strong oxycline, response time errors can be much larger (>20 $\mu$mol kg$^{-1}$) than these practical sensor uncertainties. This has notable impacts on net community production estimates (Plant et al. 2016), deoxygenation studies on isopycnals (Cervania and Hamme 2024), and assessment of optode accuracy on the BGC-Argo array (Johnson et al. 2017), clearly highlighting that there are regions where these response time errors are not insignificant. While accounting for response time errors may not be necessary in all regions of the ocean for all studies, it is still important to account for these errors in relevant regions and parts of the water column to help improve the overall performance of the BGC-Argo array. As the target accuracy and precision of the array are 1 and 0.5 $\mu$mol kg$^{-1}$, respectively, anything that can inch BGC-Argo closer to these metrics is a good step forward (Gruber et al. 2010). It is important to resolve dynamic errors in Argo data, as well as to work on resolving other issues.

This study also explored the impacts of other factors that affect a sensor's response time and performance, such as testing setup, thermal inertia effects, and foil variability. Benchtop lab experiments, using a pumped flow-through setup, highlighted the importance of considering the impacts of testing setup for practical applications. While this setup allowed for the response time of an Aanderaa 4831 optode, or more specifically the PSt3 foil used in both the Aanderaa 4330 and 4831, to be determined over a range of volumetric flow rates, the results were not practical for field applications as the setup had more complex fluid dynamics than initially thought. In the experiments changing only the temperature while keeping oxygen saturation constant, it became apparent that the assumption that the thermistor temperature is indicative of the foil temperature is not valid for the AA4330 and AA4330|WTW, but it holds for the RBR|SLOW (Fig. 11). Additionally, while it was believed that the AA4330 and RBR|SLOW both use the same PreSens PSt3 foils, an experiment where the foils were swapped between these two assets revealed that this is not the case (Fig. 12). Variability between different batches of foils was recently observed in the form of varying pressure coefficients of AA4330 optodes (Miller et al. 2024). While the PSt3 foils examined in this study appear to be, in fact, different, our experiments revealed that differences in the foils, sensor geometry, and other factors may result in different response times between the optodes.

## Comments and recommendations

Based on the results from this study, the following comments and recommendations are made for quantifying the response time of optodes and correcting measured time series:

- A great deal of care should be taken in applying the results of the laboratory studies in the field. A larger field dataset for all optode types is needed to validate the translation of response times determined in the laboratory to field response times.
- Profiling floats need to have timestamps to implement this correction, which will allow better assessment of corrections, assuming the float velocity is the local velocity around the optode.
- When characterizing the response of oxygen optodes, the entire sensor should be considered, including the foil, thermistor, sensor geometry, material, and size of the sensor.
- More work investigating consistency between batches of sensors and foils from the same manufacturer, and between the manufacturers is needed, and the additional quality control steps at the manufacturers' level to ensure consistency may be recommended.

## Acknowledgments

This work was funded by NOAA Cooperative Agreement NA19OAR4320074 for CINAR: A Cooperative Institute for the North Atlantic Region and NSF OCE# 1947567. We additionally thank Aidan Thayer for the construction of the PyroScience PICO-O2 housing and data logger and the Aanderaa pumped flowthrough system, the staff of Dalhousie Aquatron facilities for supporting the flume response time experiments, Breck Owens, Amala Mahadevan, Ersen'S Joseph, and Adam Hawkins for their insightful discussions.

## Conflicts of Interest

Mathieu Dever was employed by RBR Ltd. All other authors declare no conflict of interest.

## References

Aanderaa Data Instruments AS. 2024. "Oxygen Optode 4330W/4330/4330F Data Sheet." https://www.aanderaa.com/media/pdfs/d378_aanderaa_oxygen_sensor_4330w_4330_4330f_low_en.pdf.

Aanderaa Data Instruments AS. n.d. "Aanderaa Oxygen Optodes: Best Practices for Maintaining High Data Quality." Accessed February 17, 2022. https://www.aanderaa.com/media/pdfs/aanderaa-oxygen-optodes-best-practices-calib-info-literature-list.pdf.

Biogeochemical-Argo Planning Group. 2016. "The Scientific Rationale, Design and Implementation Plan for a

Biogeochemical-Argo Float Array." Ifremer. https://doi.org/10.13155/46601.

Bittig, H. C., B. Fiedler, P. Fietzek, and A. Körtzinger. 2015a. "Pressure Response of Aanderaa and Sea-Bird Oxygen Optodes." *Journal of Atmospheric and Oceanic Technology* 32, no. 12: 2305–2317. https://doi.org/10.1175/JTECH-D-15-0108.1.

Bittig, H. C., B. Fiedler, R. Scholz, G. Krahmann, and A. Körtzinger. 2014. "Time Response of Oxygen Optodes on Profiling Platforms and its Dependence on Flow Speed and Temperature." *Limnology and Oceanography: Methods* 12, no. 8: 617–636. https://doi.org/10.4319/lom.2014.12.617.

Bittig, H. C., and A. Körtzinger. 2015. "Tackling Oxygen Optode Drift: Near-Surface and in-Air Oxygen Optode Measurements on a Float Provide an Accurate in Situ Reference." *Journal of Atmospheric and Oceanic Technology* 32, no. 8: 1536–1543. https://doi.org/10.1175/JTECH-D-14-00162.1.

Bittig, H. C., and A. Körtzinger. 2017. "Technical Note: Update on Response Times, in-Air Measurements, and In Situ Drift for Oxygen Optodes on Profiling Platforms." *Ocean Science* 13, no. 1: 1–11. https://doi.org/10.5194/os-13-1-2017.

Bittig, H. C., A. Kortzinger, K. Johnson, et al. 2015b. "SCOR WG 142: Quality Control Procedures for Oxygen and Other Biogeochemical Sensors on Floats and Gliders. Recommendation for Oxygen Measurements From Argo Floats, Implementation of In-Air-Measurement Routine to Assure Highest Long-Term Accuracy.". Ifremer. https://doi.org/10.13155/45917.

Bittig, H. C., A. Körtzinger, C. Neill, et al. 2018. "Oxygen Optode Sensors: Principle, Characterization, Calibration, and Application in the Ocean." *Frontiers in Marine Science* 4: 429. https://doi.org/10.3389/fmars.2017.00429.

Cervania, A. A., and R. C. Hamme. 2024. "Isopycnal Shoaling Causes Interannual Variability in Oxygen on Isopycnals in the Subarctic Northeast Pacific." *Journal of Geophysical Research: Oceans* 129, no. 7: e2023JC020414. https://doi.org/10.1029/2023JC020414.

Claustre, H., K. S. Johnson, and Y. Takeshita. 2020. "Observing the Global Ocean with Biogeochemical-Argo." *Annual Review of Marine Science* 12, no. 1: 23–48. https://doi.org/10.1146/annurev-marine-010419-010956.

Dever, M., B. Owens, C. Richards, et al. 2022. "Static and Dynamic Performance of the RBRargo3 CTD." *Journal of Atmospheric and Oceanic Technology* 39, no. 10: 1525–1539. https://doi.org/10.1175/JTECH-D-21-0186.1.

Garau, B., S. Ruiz, W. G. Zhang, et al. 2011. "Thermal Lag Correction on Slocum CTD Glider Data." *Journal of Atmospheric and Oceanic Technology* 28: 1065–1071. https://doi.org/10.1175/JTECH-D-10-05030.1.

Gordon, C., K. Fennel, C. Richards, L. K. Shay, and J. K. Brewster. 2020. "Can Ocean Community Production and Respiration Be Determined by Measuring High-Frequency Oxygen Profiles from Autonomous Floats?" *Biogeosciences* 17, no. 15: 4119–4134. https://doi.org/10.5194/bg-17-4119-2020.

Gray, A. R., K. S. Johnson, S. M. Bushinsky, et al. 2018. "Autonomous Biogeochemical Floats Detect Significant Carbon Dioxide Outgassing in the High-Latitude Southern Ocean." *Geophysical Research Letters* 45, no. 17: 9049–9057. https://doi.org/10.1029/2018GL078013.

Grégoire, M., V. Garçon, H. Garcia, et al. 2021. "A Global Ocean Oxygen Database and Atlas for Assessing and Predicting Deoxygenation and Ocean Health in the Open and Coastal Ocean." *Frontiers in Marine Science* 8: 724913. https://doi.org/10.3389/fmars.2021.724913.

Gruber, N., S. C. Doney, S. R. Emerson, et al. 2010. "Adding Oxygen to Argo: Developing a Global In Situ Observatory for Ocean Deoxygenation and Biogeochemistry." https://repository.oceanbestpractices.org/handle/11329/926.

Han, F., Q. Lan, Y. Liu, et al. 2024. "Unveiling Turbulent Flow Dynamics in Blind-Tee Pipelines: Enhancing Fluid Mixing in Subsea Pipeline Systems." *Journal of Marine Science and Engineering* 12, no. 7: 7. https://doi.org/10.3390/jmse12071199.

Han, F., Y. Liu, M. C. Ong, G. Yin, W. Li, and Z. Wang. 2022. "CFD Investigation of Blind-Tee Effects on Flow Mixing Mechanism in Subsea Pipelines." *Engineering Applications of Computational Fluid Mechanics* 16, no. 1: 1395–1419. https://doi.org/10.1080/19942060.2022.2093275.

IOCCP. 2017. "EOV Specification Sheet: Oxygen." https://goosocean.org/document/.

Johnson, K. S., J. N. Plant, L. J. Coletti, et al. 2017. "Biogeochemical Sensor Performance in the SOCCOM Profiling Float Array." *Journal of Geophysical Research: Oceans* 122, no. 8: 6416–6436. https://doi.org/10.1002/2017JC012838.

Johnson, K. S., J. N. Plant, S. C. Riser, and D. Gilbert. 2015. "Air Oxygen Calibration of Oxygen Optodes on a Profiling Float Array." *Journal of Atmospheric and Oceanic Technology* 32, no. 11: 2160–2172. https://doi.org/10.1175/JTECH-D-15-0101.1.

Karstensen, J., L. Stramma, and M. Visbeck. 2008. "Oxygen Minimum Zones in the Eastern Tropical Atlantic and Pacific Oceans." *Progress in Oceanography* 77, no. 4: 331–350. https://doi.org/10.1016/j.pocean.2007.05.009.

Koelling, J., D. Atamanchuk, J. Karstensen, P. Handmann, and D. W. R. Wallace. 2022. "Oxygen Export to the Deep Ocean Following Labrador Sea Water Formation." *Biogeosciences* 19, no. 2: 437–454. https://doi.org/10.5194/bg-19-437-2022.

Lan, Q., F. Han, Y. Liu, W. Li, and Z. Wang. 2022. "Numerical Investigation on Turbulent Flow in Blind Tees." In 2022 IEEE 17th Conference on Industrial Electronics and Applications (ICIEA), 156–161. IEEE. https://doi.org/10.1109/ICIEA54703.2022.10005965.

Langdon, C. 2010. "Determination of Dissolved Oxygen in Seawater by Winkler Titration Using the Amperometric Technique." In The GO-SHIP Repeat Hydrography Manual: A Collection of Expert Reports and Guidelines, edited by

E. M. Hood, C. L. Sabine, and B. M. Sloyan, vol. 1, 18. ICPO Publication Series 134. https://doi.org/10.25607/OBP-1350.

Lautrup, B. 2011. "Boundary Layers." In Physics of Continuous Matter, 493–524. CRC Press. https://doi.org/10.1201/9781439894200-35.

Lueck, R. G. 1990. "Thermal Inertia of Conductivity Cells: Theory." *Journal of Atmospheric and Oceanic Technology* 7, no. 5: 741–755. https://doi.org/10.1175/1520-0426(1990)007<0741:TIOCCT>2.0.CO;2.

Lueck, R. G., and J. J. Picklo. 1990. "Thermal Inertia of Conductivity Cells: Observations with a Sea-Bird Cell." *Journal of Atmospheric and Oceanic Technology* 7, no. 5: 756–768. https://doi.org/10.1175/1520-0426(1990)007<0756:TIOCCO>2.0.CO;2.

Mignot, A., F. D'Ortenzio, V. Taillandier, G. Cossarini, and S. Salon. 2019. "Quantifying Observational Errors in Biogeochemical-Argo Oxygen, Nitrate, and Chlorophyll *a* Concentrations." *Geophysical Research Letters* 46, no. 8: 4330–4337. https://doi.org/10.1029/2018GL080541.

Miller, U. K., K. E. Fogaren, D. Atamanchuk, et al. 2024. "Oxygen Optodes on Oceanographic Moorings: Recommendations for Deployment and In Situ Calibration." *Frontiers in Marine Science* 11. https://doi.org/10.3389/fmars.2024.1441976.

Moat, B. I., D. A. Smeed, C. Marcinko, S. Popinet, and S. Turnock. 2016. Flow Distortion around Underwater Gliders and Impacts on Sensor Measurements: A Pilot Study Using Large-Eddy Simulations. National Oceanography Centre. https://nora.nerc.ac.uk/id/eprint/514980/.

Nicholson, D. P., and M. L. Feen. 2017. "Air Calibration of an Oxygen Optode on an Underwater Glider." *Limnology and Oceanography: Methods* 15, no. 5: 495–502. https://doi.org/10.1002/lom3.10177.

Oschlies, A. 2021. "A Committed Fourfold Increase in Ocean Oxygen Loss." *Nature Communications* 12, no. 1: 2307. https://doi.org/10.1038/s41467-021-22584-4.

Plant, J. N., K. S. Johnson, C. M. Sakamoto, et al. 2016. "Net Community Production at Ocean Station Papa Observed with Nitrate and Oxygen Sensors on Profiling Floats." *Global Biogeochemical Cycles* 30, no. 6: 859–879. https://doi.org/10.1002/2015GB005349.

PyroScience GmbH. 2024. Specifications Underwater Oxygen Sensors. https://www.pyroscience.com/en/products/all-sensors/oxcap-sub#Downloads.

RBR Ltd. 2024. "RBRcoda-T.ODO Infographic." https://rbr-global.com/wp-content/uploads/2018/11/RBRcoda-T.ODO-Infographic.pdf.

Ren, A. S., D. L. Rudnick, and A. Twombly. 2023. "Drift Characteristics of Sea-Bird Dissolved Oxygen Optode Sensors." *Journal of Atmospheric and Oceanic Technology* 40, no. 12: 1645–1656. https://doi.org/10.1175/JTECH-D-22-0103.1.

Riser, S. C., H. J. Freeland, D. Roemmich, et al. 2016. "Fifteen Years of Ocean Observations with the Global Argo Array." *Nature Climate Change* 6, no. 2: 145–153. https://doi.org/10.1038/nclimate2872.

Rolf Sonnerup, B. C. 2016. CTD Data From Cruise 33RO20161119. CLIVAR and Carbon Hydrographic Data Office. https://cchdo.ucsd.edu/cruise/33RO20161119.

Sauzède, R., H. Claustre, J. Uitz, et al. 2016. "A Neural Network-Based Method for Merging Ocean Color and Argo Data to Extend Surface Bio-Optical Properties to Depth: Retrieval of the Particulate Backscattering Coefficient." *Journal of Geophysical Research: Oceans* 121, no. 4: 2552–2571. https://doi.org/10.1002/2015JC011408.

Schlichting, H., and K. Gersten. 2017. Boundary-Layer Theory. Springer. https://doi.org/10.1007/978-3-662-52919-5.

Schmidtko, S., L. Stramma, and M. Visbeck. 2017. "Decline in Global Oceanic Oxygen Content During the Past Five Decades." *Nature* 542, no. 7641: 7641. https://doi.org/10.1038/nature21399.

Sharp, J. D., A. J. Fassbender, B. R. Carter, G. C. Johnson, C. Schultz, and J. P. Dunne. 2023. "GOBAI-$O_2$: Temporally and Spatially Resolved Fields of Ocean Interior Dissolved Oxygen over Nearly 2 Decades." *Earth System Science Data* 15, no. 10: 4481–4518. https://doi.org/10.5194/essd-15-4481-2023.

Staudinger, C., M. Strobl, J. Breininger, I. Klimant, and S. M. Borisov. 2019. "Fast and Stable Optical pH Sensor Materials for Oceanographic Applications." *Sensors and Actuators B: Chemical* 282: 204–217. https://doi.org/10.1016/j.snb.2018.11.048.

Staudinger, C., M. Strobl, J. P. Fischer, et al. 2018. "A Versatile Optode System for Oxygen, Carbon Dioxide, and pH Measurements in Seawater with Integrated Battery and Logger: A Versatile Optode System for $O_2$, $CO_2$, and pH." *Limnology and Oceanography: Methods* 16, no. 7: 459–473. https://doi.org/10.1002/lom3.10260.

Takeshita, Y., T. R. Martz, K. S. Johnson, et al. 2013. "A Climatology-Based Quality Control Procedure for Profiling Float Oxygen Data: Qc Procedure for Profiling Float Oxygen." *Journal of Geophysical Research: Oceans* 118, no. 10: 5640–5650. https://doi.org/10.1002/jgrc.20399.

Tengberg, A., J. Hovdenes, H. J. Andersson, et al. 2006. "Evaluation of a Lifetime-Based Optode to Measure Oxygen in Aquatic Systems." *Limnology and Oceanography: Methods* 4, no. 2: 7–17. https://doi.org/10.4319/lom.2006.4.7.

Thierry, V., H. Bittig, and Team, T. A.-B. 2021. Argo Quality Control Manual for Dissolved Oxygen Concentration (Version 2.1). Argo-BGC Group. https://doi.org/10.13155/46542.

Uchida, H., T. Kawano, I. Kaneko, and M. Fukasawa. 2008. "In Situ Calibration of Optode-Based Oxygen Sensors." *Journal of Atmospheric and Oceanic Technology* 25, no. 12: 2271–2281. https://doi.org/10.1175/2008JTECHO549.1.

Welty, J., G. L. Rorrer, and D. G. Foster. 2014. Fundamentals of Momentum, Heat and Mass Transfer. Wiley.

Winkler, L. W. 1888. "Die Bestimmung des im Wasser gelösten Sauerstoffes." *Berichte der Deutschen Chemischen Gesellschaft* 21, no. 2: 2843–2854. https://doi.org/10.1002/cber.188802102122.

Wirth, T., Y. Takeshita, B. Davis, et al. 2024. "Assessment of a pH Optode for Oceanographic Moored and Profiling Applications." *Limnology and Oceanography: Methods* 22: 805–822. https://doi.org/10.1002/lom3.10646.

Yang, B., S. R. Emerson, and P. D. Quay. 2019. "The Subtropical Ocean's Biological Carbon Pump Determined from $O_2$ and DIC/DI $^{13}C$ Tracers." *Geophysical Research Letters* 46, no. 10: 5361–5368. https://doi.org/10.1029/2018GL081239.

## Supporting Information

Additional Supporting Information may be found in the online version of this article.

*Submitted 26 February 2025*
*Revised 01 July 2025*
*Accepted 09 July 2025*